

Accurate Regression-based 4D Mitral Valve Segmentation from 2D MRI Slices

Dime Vitanovski^{2,3} *, Alexey Tsymbal², Razvan Ioan Ionasec¹, Andreas Greiser⁴, Edgar Mueller⁴, Xiaoguang Lu¹, Gareth Funka-Lea¹, Joachim Hornegger³, and Dorin Comaniciu¹

¹ Siemens Corporate Research, Princeton, USA

² Siemens Corporate Technology, Erlangen, Germany

³ Siemens Health Care, Erlangen, Germany

⁴ Pattern Recognition Lab, Friedrich-Alexander-University, Erlangen, Germany

Abstract. Cardiac MR (CMR) imaging is increasingly accepted as the gold standard for the evaluation of cardiac anatomy, function and mass. The multi-plan ability of CMR makes it a well suited modality for evaluation of the complex anatomy of the mitral valve (MV). However, the 2D slice-based acquisition paradigm of CMR limits the 4D capabilities for precise and accurate morphological and pathological analysis due to long through-put times and protracted study. In this paper we propose a new CMR protocol for acquiring MR images for 4D MV analysis. The proposed protocol is optimized regarding the number and spatial configuration of the 2D CMR slices. Furthermore, we present a learning-based framework for patient-specific 4D MV segmentation from 2D CMR slices (sparse data). The key idea with our Regression-based Surface Reconstruction (RSR) algorithm is the use of available MV models from other imaging modalities (CT, US) to train a dynamic regression model which will then be able to infer the incomplete information pertinent to CMR. Extensive experiments on 200 transesophageal echocardiographic (TEE) US and 20 cardiac CT sequences are performed to train the regression model and to define the CMR acquisition protocol. With the proposed acquisition protocol, stack of 6 parallel long-axis (LA) planes, we acquired CMR patient images and regressed 4D patient-specific MV model with an accuracy of 1.5 ± 0.2 mm and average speed of 1 sec per volume.

1 Introduction

Cardiac MR imaging emerges as the new gold standard for characterizing cardiac masses and the evaluation of cardiac function and anatomy. The multi-plan ability of CMR to acquire tomographic images in any plane, the capabilities to measure blood flow velocity in all three dimensions within a single slice and the non ionizing radiation gives it a significant advantage over other imaging modalities. Clinical studies have already proven that CMR is well suited for the evaluation of the complex anatomy of MV by comparing MV measurements

* Correspondence to dime.vitanovski.ext@siemens.com

extracted from CMR data with CT and US [1]. Nevertheless, the 2D slice-based acquisition paradigm of CMR limits the 4D anatomical and functional analysis of the heart by long throughput times and protracted study which can be utilized for more accurate and precise morphological and pathological analysis.

Although many works [2–4], mainly based on the seminal contribution of Cootes et al. [5] on Active Shape Models (ASM), have studied 4D chamber segmentation to overwhelm the 2D limitations of CMR, there is still no established method to extract 4D anatomical and functional information of the heart valves. Conti et al. [6] have manually initialized contours of the MV in each of the 18 radial long-axis 2D CMR slices and used interpolation to obtain a 3D model of the MV. Nevertheless, this method is characterized with long acquisition time (18 2D slices), manual initialization, a static MV model and therefore not applicable in clinical practice. On the other hand, 4D aortic and mitral valve estimated from other imaging modalities like CT and US have been introduced by [7, 8].

Within this paper we propose *a novel CMR acquisition protocol* for non-invasive assessment of the mitral valve anatomy and morphology together with *a regression-based method for patient-specific 4D MV model estimation*. Based on extensive experiments on simulated data (Section 3.1) we first defined the acquisition protocol and optimize it with respect to the number and spatial configuration of the 2D CMR slices resulting in reduced acquisition time and 4D MV segmentation error. Second, we defined the segmentation task as a regression problem (Sec. 2.1) between a full surface and a sparse one extracted from available 2D MRI slices. We solved the problem by learning additive boosting regression and its stabilization (Sec. 2.3) - bagging with random feature subsampling (BRFS) from MV models extracted from other imaging modalities (CT, US) used as a prior knowledge. Furthermore, experiments in Section 3.2 prove the concept of learning a regression model from one imaging modality and applying it into another one for 4D MV model estimation.

2 Methods

In order to accurately reconstruct the surface of MV from 2D CMR slices, we introduce a regression-based approach to surface completion. The regression problem is parameterized with the component of additive boosting regression and learned so that the most discriminative features are selected. In the training phase, we consider MV models extracted from CT or TEE US data as a output (full surface). By knowing the CMR acquisition protocol and imaging plane orientation and location with respect to the MV anatomy, we simulate the sparse CMR protocol in the corresponding CT or TEE US data and extract sparse MV surface (Sec. 2.4), considers as input (sparse surface). Once, the regression model is learned, it is utilized to estimate 4D patient-specific MV model from 2D CMR data.

2.1 Regression-based surface reconstruction (RSR)

In contrast to ASM-based methods, regression-based solutions make no implicit assumption about multivariate normality of the data. Comparing to simpler heart anatomies such as the left and right ventricle, the complex structure of MV exhibits higher variability and mesh point distributions different from normal. Thus, is more challenging to segment, especially from sparse data and requires more robust technique.

In *regression* a solution to the following optimization problem is normally sought [9]:

$$\hat{\mathcal{R}}(\mathbf{x}) = \underset{\mathcal{R} \in \mathfrak{S}}{\operatorname{argmin}} \sum_{n=1}^N L(y(\mathbf{x}_n), \mathcal{R}(\mathbf{x}_n)) / N \quad (1)$$

where \mathfrak{S} is the set of possible regression functions, $L(\circ, \circ)$ is a loss function that penalizes the deviation of the regressor output $\mathcal{R}(\mathbf{x}_n)$ from the true output, and N is the number of available training examples. In our case the reconstruction task is defined as a regression problem between the full surface model of MV and the respective sparse data acquired using the proposed CMR protocol:

$$\mathbf{y}_{surface} = \hat{\mathcal{R}}(\mathbf{x}_{sparse}) + \epsilon \quad (2)$$

In our regression problem both for input and output data we focus on shape information and ignore respective volume data. Thus, the output $\mathbf{y}_{surface}$ is always a set of m 3D points defining the MV surface:

$$\mathbf{y}_{surface} = ((x_1, y_1, z_1), \dots, (x_m, y_m, z_m))^T \quad (3)$$

2.2 Invariant Shape Descriptors

The input, \mathbf{x}_{sparse} , are shape descriptors (SD) describing the cloud of points belonging to MV in the sparse CMR data. The simplest but reliable solution is to use the coordinates of known points as input [10]. The obvious drawback of this solution is the necessity to provide point correspondence, which is not always feasible, especially for the data with high variability such as MV surface. A different solution, which we exploit here, is to use angles, distances and areas between random sampled points as point cloud descriptors [11]:

- **A3**: Measures the angle between three random points;
- **D2**: Measure the distance between two random points;
- **D3**: Measures the square root of the area of the triangle between three random points;

For the different shape descriptors proposed by [11] we measured feature importance by analysing the features selected by additive boosting. We have identified (A3, D2 and D3) to be most informative in our context with the average probability of occurrence 0.11, 0.07, and 0.13, correspondingly. In addition, all three

types are translation, rotation and scale invariant descriptors which overcome the necessity of point correspondences. Finally, histogram bins and the four first normalized central moments describing the histogram distribution are computed from the descriptors and incorporate in the regression model as input.

2.3 Ensembles of Additive Boosting Regressors

Each component m regression problem $\hat{\mathcal{R}}^m$ is solved by learning using additive boosting regression (ABR) [12]. In ABR, the weak regressors ρ_t are sequentially fit to the residuals, starting from the mean \bar{y} and proceeding with the residuals of the available set of weak regressors themselves. In ABR, the output function is assumed to take a linear form as follows [12]:

$$\hat{\mathcal{R}}(\mathbf{x}) = \sum_{t=1}^T \alpha_t \rho_t(\mathbf{x}); \rho_t(\mathbf{x}) \in \mathfrak{F} \quad (4)$$

where $\rho_t(\mathbf{x})$ is a base (weak) learner and T is the number of boosting iterations.

In the spirit of [13] and [9], we use very simple weak regressors as the base learners. These include *simple 1D linear regression* (SLR), *logistic stumps* (LS) and *decision stumps* (DS). For SLR, in each boosting iteration a feature which results in the smallest squared loss with linear regression is added to the pool of already selected features. Each weak learner is thus a simple linear regressor of the form ($y = \beta_1 x + \beta_0$) where x is the selected shape descriptor and y is a scalar output coordinate. LS is a simple logistic function on one shape descriptor x :

$$y = \frac{1}{1 + e^{-z}}, z = \beta_1 x + \beta_0 \quad (5)$$

Finally, DS is a piecewise linear threshold function where threshold θ is selected so that the variance in the subsets of instances produced is minimized. It is important to note that SLR results in a linear solution overall, while DS and LS seek for non-linear solutions.

Generalization performance improvement of the underlying regression models and avoidance of overfitting is achieved by injecting randomization in the input data and random features sub spacing (BRFS), similar to [14]. In particular, instead of providing a single model \mathcal{R} for the training set X , we generate a set of models \mathcal{R}_i^j , each obtained using the same additive regression procedure but on a *random sample* of the data, with instances S_i obtained using random sampling with replacement, and a subset of features F_j including 50% features randomly sampled without replacement from the original set. The final solution is then simply the mean surface for the surfaces obtained with the regressors generated from the random samples: $\mathcal{R} = \text{mean}_{i,m}(\mathcal{R}_i^m)$.

2.4 Mitral Valve Model Estimation from 2D CMR Slices

The mitral valve, located between the left atrium and the left ventricle, includes *posterior leaflet* composed by the posterior leaflet tip, posterior and an-

terior commissures and the postero annular midpoint, *anterior leaflet* defined by anterior leaflet tip, the left/right trigone and two commissures, *annulus*, *free edge*. Point distribution model (Fig. 1(left)) is used to represent the mitral valve surfaces S_{MV} in the \mathbf{u} and \mathbf{v} direction ($\mathbf{S}_{posterior}(u, v) = (31, 17)$, $\mathbf{S}_{anterior}(u, v) = (27, 17)$).

Annulus and Free Edge detection. Similar to [15] we define our joint context landmark set between the posterior annulus and the free edge landmarks (PA, PFE) and the anterior leaflet (AA, AFE), respectively (Fig.1(middle)). On each 2D LAX CMR slice we apply 2D landmark classifiers, trained with PBT [16] and 2D Haar-like features to detect the annulus and free edge landmarks independently. From the candidates generated by the detectors we select the top M candidates for the annulus detection and the top N candidates for the free edge detection. In the second stage the joint context is build from all possible candidates' pairs $\langle \text{annulus plane}, \text{free edge plane} \rangle$. In the final stage a context operator C is applied to compute Haar-like features from the set of all possible candidates used to train a joint context classifier for MV landmark detection.

Mitral valve contour estimation. From previously detected landmarks we initialize the contours, parameterized by 17 discrete points, as a straight line and search for edges along the normals. However, this method is not sufficient for accurate contour estimation and therefore further manual refinement is usually required.

Regression-based full 4D MV surface reconstruction. In this step shape descriptors - SD are computed from the landmarks and contours detected from the 2D CMR slices in each cardiac frame (t) and incorporated into the trained regression model as input. As a result, full dynamic MV model is estimated in the 2D MRI slices(Fig.1(right)).

$$S_{MV} = \mathcal{R}(SD(\text{landmarks}, \text{contours})) \quad (6)$$

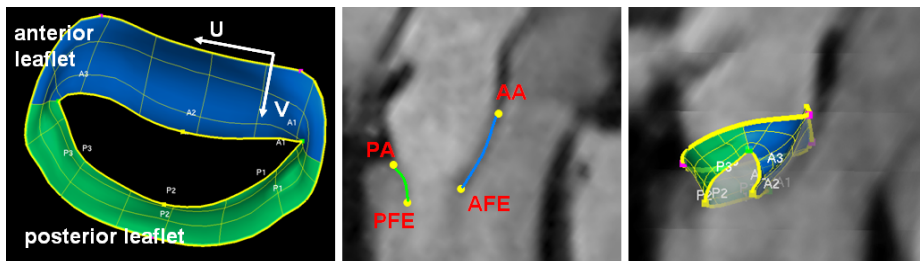


Fig. 1. *Left:* MV model. *Middle:* MV landmarks and contours. *Right:* MV model regressed into the patient-specific CMR anatomy

3 Experimental Setting and Results

3.1 MRI Acquisition Protocol Definition

CMR scanner (1.5T) with phased-array receiver coil and breath-hold acquisition was used to acquire cine images for MV function analysis. Full cardiac cycle was covered by using a retrospectively/prospectively gated ECG signal. Data were collected during a breath-hold (8 heart beats, slice thickness 4.5 mm, echo time 1.39 ms, pixel bandwidth 925 Hz, matrix 208×124 , excitation angle 59° , field of view 276mm-340mm).

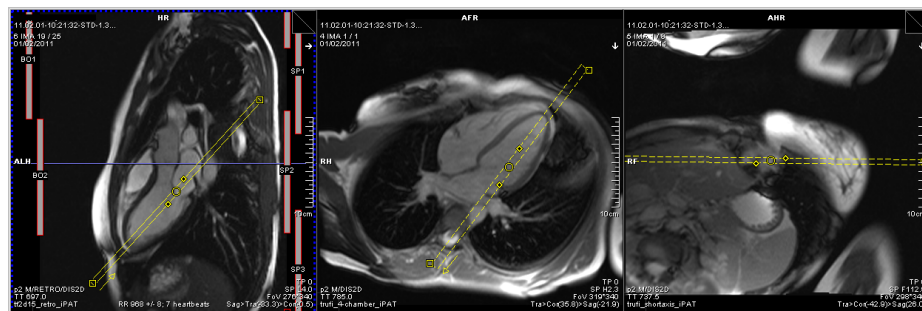


Fig. 2. Mitral valve acquisition protocol. *Left:* three-chamber view. *Middle:* four-chamber view. *Right:* short-axis view

The mitral valve imaging plane was defined by acquiring four-chamber, three-chamber and short-axis view in the diastolic phase of the cardiac cycle (see Fig. 2). Initial orientation of the imaging plane is given by the short-axis view, where the plane passes through the MV commissures. Subsequently, parallel slices were defined perpendicular to the MV annulus in the four- and three-chamber views.

In order to find the best trade-off between MV segmentation error and acquisition time the CMR imaging protocol was defined based on simulated data. The imaging plane was placed as illustrated in Fig. 2 in 200 US TEE studies and used to obtain sparse images. To make the simulation more realistic we add noise to the plane location and orientation. The regression-based surface reconstruction method as introduced in Section 2.1 and Section 2.4 was applied to segment the MV from the simulated sparse images in the end-diastolic (ED) and end-systolic (ES) phase of the cardiac cycle.

Based on the experiments from the simulated data (see Table 1) a stack of 6 parallel LA planes results in best trade-off between MV segmentation error and acquisition time (4.86 min for very experienced user). A protocol with 6 radial LA planes was also considered as an option. However, due to the long acquisition planning time, the complicated plane settings and the plane misregistration characteristic for this acquisition protocol, we found that a stack of parallel planes is more appropriate for MV segmentation.

No. Planes	2	3	4	5	6	7	8	9	10
ED	6.7 ± 1.1	5.6 ± 1.0	4.4 ± 0.9	3.5 ± 0.68	3.1 ± 1.1	2.6 ± 1.0	2.3 ± 1.0	2.1 ± 1.0	1.8 ± 0.86
ES	2.9 ± 1.2	2.6 ± 2.2	2.2 ± 1.5	2.1 ± 1.4	2.1 ± 1.2	2.3 ± 1.6	2.5 ± 2.3	2.1 ± 1.1	1.9 ± 1.0

Table 1. MRI Protocol definition

3.2 Mitral Valve Surface Reconstruction

The proposed framework for personalized 4d MV model estimation in sparse data was evaluated on a large set of simulated data (200 US TEE and 20 cardiac CT sequences) and on *2 prospectively and retrospectively ECG gated CMR studies acquired according to our protocol* as introduced in Section 3.1. Each volume in the data set is associated with annotation, manually generated by experts, which is considered as ground truth. A mesh-to-mesh error was used for the evaluation of all presented results for the ED phase which is considered to be the most difficult phase for model estimation (valve is opened).

Intra and inter modality accuracy of our RSR method with respect to different weak learners was evaluated. The inter modality accuracy was evaluated by training the regression model on images simulated from US TEE data and tested on simulated sparse images from CT data. For the intra modality accuracy a 3-fold cross validation was used to divide the US TEE data set into training (used to train the regression model) and test data (used to evaluate the reconstruction error).

Table 2 summarizes the patient-specific MV surface reconstruction error from incomplete data for the best CMR plane configuration protocol: stack of 6 parallel planes. We also show how different types of weak learners (simple 1D linear regression - **SLR**, logistic stump - **LS** and decision stump - **DS**) influence the reconstruction error and how this error can be reduce by incorporating all three weak learners into the framework of bagging with random feature sub-sampling (**BRFS**). Each additive boosting regression model includes 100 weak regressors with 0.2 shrinkage. For BRFS, 10 bootstrap samples of examples were generated, each with 10 random feature subsets including 50% original descriptors (resulting in 100 additive boosting regression models to combine).

mm	SLR	LS	DS	BRFS	mm	SLR	LS	DS	BRFS
no noise	1.7 ± 0.7	1.8 ± 0.9	2.1 ± 0.9	1.6 ± 0.4	no noise	2.2 ± 0.6	2.5 ± 0.6	2.9 ± 1.0	1.6 ± 0.6
2mm noise	1.8 ± 0.4	1.9 ± 0.7	2.3 ± 1.5	1.8 ± 0.7	2mm noise	2.6 ± 1.2	2.5 ± 0.7	3.1 ± 1.0	1.8 ± 0.8
3mm noise	2.0 ± 0.6	1.9 ± 0.5	3.0 ± 3.1	1.9 ± 0.5	3mm noise	3.0 ± 1.3	3.5 ± 1.0	3.8 ± 0.9	2.3 ± 0.5

Table 2. Left: Intra modality RSR accuracy (US). **Right:** Inter modality RSR accuracy (Train on US, reconstruct in CT)

With the results of the inter modality accuracy and the clinical studies which prove the compactness of the MV anatomy between different imaging modalities[1], we have shown that a regression model can be learned from one imaging

modality (US) and used to estimate a patient-specific MV model in other imaging modality (CT). Finally, the regression model was learned offline with BRFS on all available US and CT data (1295 3D volumes) and evaluated on the CMR studies acquired according to the proposed protocol. A surface reconstruction error of 1.5 ± 0.2 mm was achieved within 1 sec per volume for the retrospectively and prospectively ECG gated CMR studies. Figure 3 illustrates the estimated MV models for the ED and ES phase of the cardiac cycle for the CMR studies.

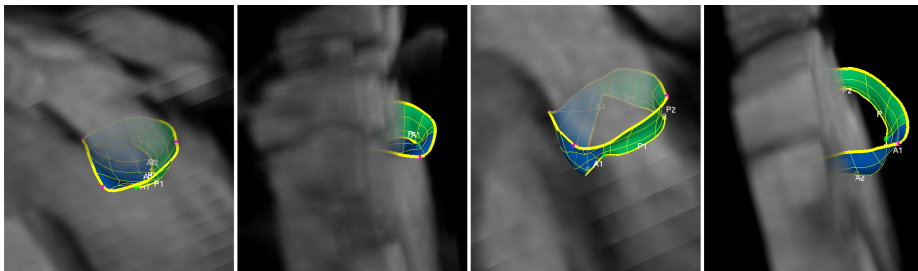


Fig. 3. Examples of the estimated MV model in the ED and ES phase for the prospectively and retrospectively acquired CMR studies

4 Conclusion

This paper presents a novel CMR acquisition protocol for fast non-invasive 4D anatomy and function assessment of the mitral valve. A regression-based surface reconstruction (RSR) method, designed according to the protocol, is used to learn from the existing MV models in US and CT data and applied to estimate patient-specific 4D MV model from sparse CMR data. With our protocol and method we overcame some of the CMR limitations: long through-put time, protracted study, 2D function and anatomy analysis. Furthermore, a 4D model of the MV can be utilized to extract more accurate morphological and pathological information over the cardiac cycle. Extensive experiments on simulated (CT and US) data have proven our concept of learning a regression model from one modality (US) and applying it on other one (CT) for 4D MV surface reconstruction. Following this concept we learn the RSR algorithm on all available CT and US data and demonstrate a reconstruction accuracy of 1.5 ± 0.2 within 1 sec pro volume for the CMR studies.

References

1. Djavidani, B., et al.: Planimetry of mitral valve stenosis by magnetic resonance imaging. In: American College of Cardiology. Volume 45. (2005) 2048–2053
2. van Assen et al., H.C.: Spasm: a 3d-asm for segmentation of sparse and arbitrarily oriented cardiac mri data. In: Medical Image Analysis. (2006)

3. Frangi, A.F., et al.: Threedimensional modeling for functional analysis of cardiac images: A review. In: IEEE Trans. Medical Imaging. Volume 20. (2001) 2–25
4. Wang, X., et al.: Reconstruction of detailed left ventricle motion from tmri using deformable models. In: FIMH. (2007)
5. Cootes, T.F., et al.: Active shape models-their training and application. In: Computer Vision and Image Understanding. Volume 61. (1995) 38–59
6. Conti, C.A., et al.: Mitral valve modelling in ischemic patients: Finite element analysis from cardiac magnetic resonance imaging. In: Computing in Cardiology. (2010)
7. Ionasec, R., et al.: Patient-specific modeling and quantification of the aortic and mitral valves from 4d cardiac ct and tee. In: TMI, in press (2010)
8. Grbic, S., et al.: Complete valvular heart apparatus model from 4d cardiac ct. In: MICCAI. (2010)
9. Zhou, S.K., et al.: Image based regression using boosting method. In: ICCV. (2005)
10. Vitanovski, D., et al.: Cross-modality assessment and planning for pulmonary trunk treatment using ct and mri imaging. In: MICCAI. (2010)
11. Osada, R., et al.: Shape distributions. ACM Transactions on Graphics **21** (2002) 807–832
12. Friedman, J.H.: Greedy function approximation: A gradient boosting machine. Annals of Statistics **29** (2000) 1189–1232
13. Viola, P., Jones, M.: Rapid object detection using a boosted cascade of simple features. In: CVPR. (2001)
14. Webb, G.I.: Multiboosting: A technique for combining boosting and wagging. In: Machine Learning. (2000) 159–196
15. Lu, X., et al.: Discriminative joint context for automatic landmark set detection from a single cardiac mr long axis slice. In: FIHM. (2009)
16. Tu, Z.: Probabilistic boosting-tree: Learning discriminativemethods for classification, recognition, and clustering. In: ICCV. (2005)